Stochastic finite-fault ground-motion simulation in a wavefield diffusive regime: case study of the Mt. Vesuvius volcanic area.

D. Galluzzo[(1)], G. Zonno[(2)], E. Del Pezzo[(1)]

[(1)]Istituto Nazionale di Geofisica e Vulcanologia, Sezione di Napoli "Osservatorio Vesuviano", Italy

[(2)]Istituto Nazionale di Geofisica e Vulcanologia, Sezione di Milano-Pavia, Italy

Abstract

The main aim of the present work consists in the validation of stochastic method for simulating weak ground motion in a diffusive regime due to low-to-moderate magnitude earthquakes, and in particular in its application to a volcanic area. We simulated the peak ground acceleration and the response acceleration spectra caused by two earthquakes scenarios (M_D = 4.3 and M_D = 5.4) at Mt. Vesuvius volcanic area by using the stochastic finite-fault simulation method. We validated the stochastic methodology by combining source, path and site parameters of the investigated area considering the time duration parameter, T_{rms}, calculated on the study seismograms. The values of time durations are confirmed by calculating the same parameter, T_{rms}, on the seismogram energy envelope described by multiple scattering models, in terms of scattering and the intrinsic dissipation coefficient. Initially, the simulations were evaluated for 10 local earthquakes ($1.7 \leq M_D \leq 3.6$) that occurred at Mt Vesuvius in 1999 and are then compared with the observed data. The comparison between simulated and observed seismograms has been used to calibrate the stochastic procedure, and has been considered as the starting point for simulating ground motion for the scenario earthquake ($M_D > 3.6$) that could occur in the study area. The scenario earthquake and the relative fault features were chosen on the base of statistical, tectonic, structural and historical studies of the study area. We simulated ground motions for a maximum magnitude value, M_{max}, of 4.3, determined from examination of the Gutenberg-Richter law for the study area, and also for an M_{max} = 5.4, a magnitude that is associated with the earthquakes that struck the ancient town of Pompei 17 years before the eruption of Mt Vesuvius that occurred in 79 AD. The largest values of A_{max} for the M_D = 4.3 seismic event are in the range of 0.140 g to 0.029 g. In the case of M_D = 5.4, we obtain PGA values in the range between 0.17 and 0.55 g.

Keywords: Stochastic finite-fault modeling; ground-motion simulation; response acceleration spectra; time duration; diffusion process, Mt Vesuvius.

1. Introduction

Mt Vesuvius is potentially one of the most dangerous volcanoes in the World. The Civil Protection Agency in Italy has developed evacuation plans in case of reactivation of its volcanic activity. In the last revision of these plans, attention was also paid to possible local volcano-tectonic earthquakes of moderate magnitude that might accompany any future eruption and could produce local damage to infrastructures, including the evacuation routes. The Italian Civil Protection Agency has therefore requested estimations of the maximum acceleration (A_{max}) that would be produced by the local seismic input to be expected in the area. This value of A_{max} may well be different from that indicated by the seismic hazard map that has already been prepared for the whole of the Italian territory, as that map (http://esse1-gis.mi.ingv.it) was prepared using the available catalogue of the seismicity in Italy as input, in which no earthquakes of significant magnitude are reported to be associated with eruptions of Mt Vesuvius.

To fulfill this request, we have calculated the maximum acceleration, A_{max}, and the response acceleration spectra with 5% damping, hereafter called simply "response spectra", in the territory around Mt Vesuvius. We used the stochastic method [hereafter indicated as SM] based on the approximation of finite rectangular fault (Beresnev and Atkinson, 1997). This technique has been used for the estimation of the peak parameters of ground motion in many regions of the World (Akinci et al., 2001; Atkinson et al., 2002; Berardi et al., 2000; Carvalho et al., 2001, 2007; Castro et al., 2001) and it is particularly useful for the simulation of ground motion in the frequency range usually investigated in earthquake engineering [1 – 10 Hz]. In this approach, the high frequency part of the seismic signal can be treated as a random function. For the application of the SM, the ground motion duration in the area needs to be known, as a function of distance and magnitude. Here, we calculate the empirical relationship between duration and distance from experimental data; in addition, we validate this empirical relationship through theoretical considerations based on the theoretical energy envelope calculated in a diffusive regime. The approach is similar to that followed by Pousse et al. (2006) who applied the stochastic approach by Sabetta and Pugliese (1996) to the K-net Japanese Database improving the method by considering the time envelope of the accelerogram based on empirical models.

Our procedure essentially consists of two steps. The first is related to the calibration of area-specific parameters and to the validation of the method by comparing the observed seismograms and response spectra with those obtained through simulation. The second step consists of simulating the maximum acceleration and response spectra for the expected local, maximum-magnitude earthquake.

In the next sections we will first give an introduction to the tectonic setting of the Mt Vesuvius area. We will describe the dataset used for calibrating the SM and we will discuss how the

expected magnitude has been evaluated. In the subsequent paragraphs, the keypoints of the stochastic technique will be shown and the details of calibration procedure used in this work will be described together with the model parameters used for the area under investigation. A detailed and quantitative description of the results (maximum acceleration, A_{max} , and response spectra) and the relative discussion will conclude the work.

2. The Mt Vesuvius volcanic area: tectonic setting and background seismicity

Somma Vesuvius is a composite central volcano located in the Campania Plain near the suburbs of the city of Naples. It is formed by an ancient caldera (Mt Somma) and a younger cone (Mt Vesuvius). The Somma structure is composed of lava flows and minor scoria-fall deposits. The structure of the Somma-Vesuvius volcanic complex has been studied by the integration of mesostructural measurements, focal mechanisms and shear-wave splitting analyses (Bianco et al., 1998). Fault-slip and focal mechanism analyses indicate that the volcano is affected by NW-SE, NE-SW oriented oblique normal slip faults and by E-W oriented normal faults. The NW-SE oriented oblique slip-fault system represents the main discontinuity on which the volcano lies (Bianco et al., 1998).

The past eruptive activities of Mt Vesuvius have caused great damage to the surrounding towns. The last eruption occurred in 1944. At present, the seismic activity of Mt Vesuvius is characterized (Del Pezzo et al., 2004) by a low level of seismicity (a few hundred micro earthquakes per year) and by poor fumarolic activity located inside the caldera rim. The last seismic swarm occurred in 1999 with a maximum duration magnitude, M_D , of 3.6, the greatest M_D observed since the last eruption in 1944.

3. Data Set

The data set is composed of 10 low-to-moderate magnitude earthquakes ($1.7 \leq M_D \leq 3.6$) located at depths between 1.4 km and 4.0 km b.s.l (Table 2). The selection of these events was made according to two requirements: earthquakes with: 1) well-known focal mechanisms and records with good signal-to-noise ratios; and 2) the largest duration magnitudes and hypocentral distance range. The second of these arises from the need to validate the stochastic procedure on the largest range of distance and duration magnitudes available. The epicenter distribution of this data set is shown in Figure 1. We have used waveforms recorded at the BKE, FTC and SGV digital stations, to compare the synthetic with the observed seismograms. The waveform recorded at these stations are representative of the whole available data set in terms of propagation media (hypocentral distance range and attenuation properties) and local site condition. The source-site

distance ranges from 2 to 6 km and the site conditions are representative of the local geological characteristic for the summit part of the volcanic complex for SGV ad BKE and of its base for FTC site. Taking into account these features, we checked the stochastic procedure on the waveforms recorded at these three sites and considered the result as a significant indication for the extension of the method to all the other stations.

BKE, SGV and FTC stations were equipped with digital station gain-ranging PCM 5800 Lennartz (12 bit) with MARK L4C 3-component sensors (proper frequency = 1 Hz; damping = 0.7; sensitivity G = 169 V/m/s). The digital stations sampled seismic signals at 125 Hz, with a low-pass, anti-alias filter at a cut-off frequency of 25 Hz. All of the velocity seismograms available were corrected for instrument response and differentiated in the time domain to obtain the equivalent acceleration signals.

The locations, magnitude and focal solutions for the 10 events used in this study were taken from the literature (Del Pezzo et al., 2004), as indicated in Table 2 and will be described in sub-section 5.3.

4. Application of the method to the Mt Vesuvius area: the expected maximum magnitude event

Following a preliminary study based on a point source stochastic simulation of the ground motion at Mt Vesuvius (Galluzzo et al., 2004), we improved the estimation of the maximum acceleration and response spectra generated by local volcano-tectonic earthquakes using finite-fault stochastic simulation. In this approach we simultaneously take into account finite source, propagation parameters and local site effects of the study area. One of the most important aspects in the evaluation of A_{max} is the evaluation of the largest seismic event and the corresponding maximum magnitude, M_{max}.

The maximum magnitude of an earthquake in a given region is a crucial parameter in the evaluation of seismic hazard. It can be estimated (1) from a consideration of the maximum fault area that can rupture in a single event; (2) by the magnitude truncation in the seismicity seen for source zone in which the return period for the maximum magnitude is shorter than the observation period (Basham et al., 1982); or (3) by a statistical study of the seismic catalogue (Kagan, 1997).

In the present work, we choose two different values of M_{max} based on the instrumental seismicity and on the historical data respectively. The values of M_{max} evaluated on the base of historical seismicity (M_{max} = 4.1 ± 0.2) were estimated in terms of M_D for a return period of 30 years, using the Gutenberg-Richter frequency-magnitude relationship (hereafter indicated as G&R) as discussed in Galluzzo et al. (2004). Taking this into account, we assume an M_{max} equal to 4.3. This is close to some of the M_{max} values seen during pre-eruptive phases of some volcanoes around

the world (Benoit and McNutt, 1996) and corresponds to the values reported by Festa et al. (2003) and Cubellis et al. (2007) based on instrumental seismicity data for Mt Vesuvius. Furthermore, on the base of historical data, Cubellis et al. (2007) indicated two energy levels associated with the M_{max}: a lower level associated with an M_{max} = 4.5 (related to the activation of the whole seismogenetic structure detected over the past 40 years of seismicity) and an upper level associated with an M_{max} = 5.4 (on the basis of historical considerations relating to the earthquake that occurred in 62 AD, before the big Pompei eruption). As already discussed, we assumed that the M_{max} = 4.3 event is associated with a return period equal to 30 years; it is difficult to estimate a return period for M_{max} = 5.4, due to the limitation of the seismic catalogue. However, historical studies (Cubellis et al., 2007) have shown that earthquakes with a magnitude larger than 4.3 occurred more than 2000 years ago. Thus, we arbitrarily assumed a return period of 2000 years for M_{max} = 5.4.

The dimensions of the faults that could generate seismic events with respectively M_D = 4.3 and 5.4 were calculated using the Wells and Coppersmith (1994) relationship, which links the dimension of the fault to the magnitude of the target event in the assumption $M_D = M_W$ (Montaldo et al., 2005). On the basis of these relationships, we set an M_D= 4.3 fault plane area of 4.0 km^2 and an M_D= 5.4 fault plane area of 32.0 km^2. The orientation and geometric features of the fault that could reasonably be activated in the case of an eruption were deduced through a detailed structural and geophysical study of the Somma-Vesuvius volcanic complex, based on mesostructural measurements, focal mechanisms and shear-wave splitting analyses. At regional scale, the Somma-Vesvius Mesozoic basement is affected by SW-dipping faults and Northeast-Southwest-trending faults. Other minor structures (aligned scoria cones, fractures and minor faults) are also present on the surface and affect the north-eastern and north-western sector of the Somma edifice, where the fractures trend in NW-SE and NE-SW direction (Bianco et al., 1998). Shear-wave splitting analysis reveals an anisotropic volume due to stress induced cracks NW-SE aligned by faulting process and the authors identified NW-SE trending oblique-slip fault system as the main discontinuity on which the volcano lies. Unfortunately, in literature there are no estimates of the real dimensions of these fault structures; consequently the determination of M_{max} using the empirical relation between fault size and magnitude is impossible. Thus, we have taken from the study of Bianco et al. (1998) the information about fault strike and dip, and estimated the fault size by the presumed M_{max} .

On the basis of these results, we selected a fault structure that intersects the crater, with a strike angle of 135° (NW-SE orientation) and a dip angle of 60° and assumed that this earthquake share the same hypocenter of the M_D = 3.6 earthquake occurred in 1999 and is located in the middle of the fault plane (Lat. 40° 49’ 52’’ N, Long. 14° 25’ 52’’ E; depth 4.0 km b.s.l). In addition, fault geometry and size were evaluated for an M_D = 5.4 earthquake. We assumed that the fault surface (8 x 4 km^2) intersects the crater along a NW-SE orientation (strike = 135°; dip = 60°) and that its nucleation point coincides with that of the M_D = 4.3 event and is located in the middle of the fault

plane. The geometrical features and the location of the nucleation point related to the two earthquake scenario are shown in table 1.

We note here that alternative scenarios not considered by the present study may include other possible fault systems related to the renewal of volcanic activity.

5 Procedure of the analysis

Ground motion shaking and response acceleration spectra in the volcanic area of Mt Vesuvius were calculated using the stochastic finite fault approach and implemented in the FINSIM code (Beresnev and Atkinson, 1998a). The first step is the calibration of the method. This target was reached through the following analysis procedure:

- selection of digital records of 10 local earthquakes related to those that occurred during the seismic crisis in 1999, where the strongest had a magnitude $M_D = 3.6$;
- processing of velocity records to obtain accelerograms and response spectra (5% damping) using the appropriate instrumental corrections;
- estimation of the size of the fault starting from the relationships developed by Wells and Coppersmith (1994) assuming M_W equal to M_D;
- estimation of time durations (T_{rms}) from records following the procedure described by Gusev (1983). There is a discussion on how all of these parameters were obtained in section 5.2;
- application of the stochastic finite fault simulation technique to calibrate the parameters of the model using the "trial and error" approach by fitting the recorded with simulated site corrected response spectra and the observed waveforms with the site corrected synthetic waveforms; a trial and error procedure is used to infer the stress drop value, $\Delta\sigma$, and the sub-fault size, dl. We provide frequency dependent site effects estimated for the target sites, as well as an average Q value for the region.

The previous procedure was used to calibrate the SM discussed in the following section 5.1. Finally, the evaluation of response acceleration spectra (PSA) in the frequency range [1-30 Hz] and PGA for the possible largest events of $M_D = 4.3$ and $M_D = 5.4$ was made by using the previously validated stochastic finite-fault method.

5.1 Finite-fault ground simulation

We used the procedure described by Beresnev and Atkinson [1997, 1998b] that generalizes the stochastic simulation technique proposed for point sources by Boore [1983, 2003] to the case of

finite faults. The fault plane was assumed to be rectangular, and was subdivided into an appropriate number of sub-faults, which were modeled as point sources characterized by an ω^2 spectrum.

The rupture front that spreads radially from the nucleation point triggers the sub-faults when it reaches their center; the sub-fault acceleration time histories are propagated to the observation point by considering specified distance-duration curves and attenuation model. The sub-fault moment and corner frequency are derived from the size of each cell, and the number of sub-faults triggered is adjusted to reach the specified target moment. A random component is included in the sub-source trigger times to account for the complexity in the ground motion generation process. The corner frequency of the ω^2 spectrum is related to the sub-fault size Δl, to z, a parameter related to the sub-fault radiation amplitude, and to y, the fraction of rupture propagation velocity to shear wave velocity, β. The amplitude of sub-fault radiation is proportional to the quantity z^2, with z=1.68 for "standard" ruptures (Beresnev and Atkinson, 1997). The method has been applied to events with moment magnitude M_w, lower than 4.0 (Motazedian and Atkinson, 2005a) and in principle can be used in any tectonic environment, due to the flexibility in the specification of the input parameters, which include models of distance-dependent sub-source duration, geometric spreading and intrinsic Q(f) attenuation. Slip distribution on the fault plane and two separate amplifications can also be specified, in order to account for crustal amplification and local site effects.

The limitations of the stochastic method used in this work are mainly related to the assumption of a constant radiation pattern and to its inadequacy to simulate low frequency directivity effect. Recently, Castro et al. (2006) have simulated strong motion seismograms by using frequency-dependent radiation pattern coefficient for Umbria-Marche (Central Italy) earthquake of M_w= 6.0 and have compared the results with those obtained by technique of Beresnev and Atkinson (1997,1998b) used in the present work. They found a reduction of the fitting errors on acceleration spectra of about 9% and estimated that site and directivity effects are more relevant respect to those associated with radiation pattern. Another limitation of FINSIM is to not take into account the low frequency directivity effect; recently, Motazedian and Atkinson (2005b) improved the method by considering a dynamic corner frequency to simulate directivity effect and a reduction of errors equal to 24% on observed spectra was found (Castro et al., 2007) using this improvement. Other hybrid method for taking into account these features were proposed by Pulido and Kubo (2004) who combined a deterministic simulation of wave propagation for low frequencies and a semi-stochastic modeling approach for high frequencies.

In the present work we considered that the influence of radiation pattern and directivity could be not critical for the FINSIM simulations of low magnitude accelerograms, where the high frequency content play a predominant role in the observed spectra. This last statement can be questionable for the M_D=5.4 earthquake scenario, where the dimension of the fault are larger than the hypocentral distance. However, also in this last case, the uncertainties on ground motion

parameters due to the errors on model parameters are less than 35% (Sorensen et al., 2007). Moreover, they are comparable with the uncertainty associated with the assumption of absence of directivity effects.

5.2 Model Parameters

The modeling parameters used for the simulations in this work are shown in Table 3. The seismic moment M_0 was evaluated by applying the relation between duration magnitude M_D and seismic moment M_0 calculated by Del Pezzo et al. (2004) for Mt Vesuvius:

$$\log M_0 = 9.8 + 0.8 \cdot M_D \qquad (1)$$

where seismic moment M_0 is expressed in N·m. The fault plane dimensions and orientation were evaluated, respectively, by the relationship of Wells and Coppersmith (1994) and by the focal mechanisms reported by Del Pezzo et al. (2004). The hypocenters were assumed to be located at the centers of the faults and a random distribution of slip on the fault plane was assumed. Indicative stress drop values were taken from the work of Galluzzo et al. (2006) and the final values were obtained with the trial and error procedure defined before, changing the value of stress drop. The average value of shear wave velocity was calculated from the high resolution tomography carried out by Scarpa et al. (2002). Average density value was deduced from the work of Zollo et al. (2002). Attenuation parameters were taken from Del Pezzo et al. (2006a, 2006b). We assumed parameter Q constant with frequency and took into account the average value of Q evaluated on the high resolution 3D model of S-wave attenuation for the volcanic structure by Del Pezzo et al. (2006a, 2006b). The high frequency content of the simulated ground motion was also controlled by the cut-off frequency f_{max}, beyond which the acceleration spectrum decay sharply with increasing frequency (Pulido and Kubo, 2004). In the present paper we do not observe any change in the spectral decay beyond the corner frequency till to the cut-off frequency (25 Hz) of the anti-alias filter. Consequently, we can reasonably assume that $f_{max} \geq 25$ Hz. For practical reasons, we set $f_{max} = 20$ Hz. Site effect transfer functions for each of the investigated sites were obtained by Galluzzo et al. (2006), where the site effect were evaluated from local low-to-moderate earthquakes ($1.7 \leq M_D \leq 3.6$) by applying direct spectral ratios, generalized inversion method on S-wave and generalized inversion method on coda waves (Fig. 2). The authors found a good agreement between the results obtained with different techniques, and observed the highest amplification level above 8 Hz for the station located on the summit part and below 8 Hz for the station located in the lower part of the volcanic complex.

The other crucial aspect for an optimal application of the procedure is the precise knowledge

of the relationship between duration and source-site distance. In facts, the strong motion duration parameter can have a strong influence on earthquake damage. A motion with moderate amplitude but long duration may produce enough load reversals for damaging responses to build up in a structure (Kramer, 1996). Generally this task is passed over using empirical relationships typical of the area under study (Beresnev and Atkinson, 1997). Less crucial, but anyway important, is how the duration is defined and hence measured. Bolt (1973) evaluated the strong motion duration by considering the "bracketed duration", in which the amplitude of acceleration was greater than 0.05 g. The Trifunac and Brady (1975) approach consists of integrating the squared amplitude of the record and taking the time interval between 5% and 95% of total cumulative energy. Gusev (1983) proposed the use of the rms duration, T_{rms}, defined by considering the power moments of the squared amplitude of the signal. This definition of time duration was applied by Petukhin and Gusev (2003) for small local earthquakes occurred in Kamchatka region. Kawashima et al. (1985) considered as time duration the temporal segment in which the amplitudes exceed some fraction of the peak value.

In this study we applied the procedure following Gusev (1983) by evaluating T_{rms} on 54 waveforms from 28 local earthquakes ($1.7 \leq M_D \leq 3.6$) occurred in 1999 and recorded at the sites of interest. Interestingly, we noticed a coincidence (within an uncertainty of 1s) of the empirically calculated durations at different distances, with those theoretically evaluated applying the definition of Gusev (1983) to the theoretical envelope of the seismograms; the theoretical envelope was calculated on the basis of the diffusion model (Sato and Fehler, 1997) (Fig. 3). This model describes the energy envelope of the entire seismogram as a function of the lapse time and of the parameters characteristic of the medium (the diffusivity and the intrinsic attenuation coefficient). The comparison provides the engineering seismology community with an improvement of the ordinary stochastic method, adding the information obtained from coda wave studies. For this purpose, we used the experimental results obtained by Del Pezzo et al. (2006a), who measured diffusivity and intrinsic attenuation for the area of Mt Vesuvius. The details of this application are described in the Appendix. Furthermore, the empirical relationship between ground motion duration and hypocentral distance is plotted in Figure 4. Assuming a linear relationship between T_{rms} and distance, we applied a least square fitting procedure to obtain the following relationship:

$$T_{rms} = 0.9 \cdot R + 1.5 \qquad (2)$$

where R is the hypocentral distance in kilometers, and T_{rms} is the time duration in seconds. The uncertainties associated with the parameters in equation (2) (20% of calculated values) give an error of 0.4 s on the estimation of T_{rms}.

6. Results of the simulation

The SM is calibrated by the experimental parameters obtained using the digital records. We used 10, 3 and 2 recorded waveforms, recorded respectively at BKE, SGV and FTC. Examples of the stochastic simulations compared with the observed waveforms at the BKE and SGV stations are shown in Figures 5-8. The fit was obtained using the "trial and error" procedure described in sub-section 3.2. The simulated response spectra (at 5% damping) shown in the grey filled curves were obtained by calculating the average response spectra over 30 stochastic simulations. These values were evaluated by considering the average values from 30 simulations.

The results obtained comparing the simulated and recorded waveforms at station BKE are summarized in Table 4, with good agreement seen between the durations of the simulated and observed waveforms and between the maximum accelerations: the differences between observed maximum accelerations (column V) and the simulated ones (column VI) lay within one standard deviation. In addition, the stress-drop values for which the best fit was reached (column IV of Table 4) are similar to those evaluated experimentally (Galluzzo et al., 2006): local earthquakes with an M_D in the range of 1.7 to 3.3 are characterized by stress-drop values that are equal or less than 10 bar; and the 3.6 M_D event shows a stress-drop value close to 50 bar. The high value of the stress drop found for the highest magnitude earthquake can be explained by the greater tectonic stress that is released in the pre-fractured carbonate basement with respect to that characteristic of the shallower and more unconsolidated materials, that make up the volcanic edifice (Del Pezzo et al., 2004). An important issue for the application of SM consisted in the choice of the subfault size Δl. Δl is related a) to the total number of subfaults, b) to the amplitude of summed radiation from each subfault and c) to the corner frequency of subfault spectrum (Beresnev and Atkinson, 1998a). The most remarkable effect of changing Δl value is the increasing of the response spectra frequency content for decreasing subfault dimension Δl. By applying "trial and error" procedure, subfault dimension Δl for the selected seismic events were let to vary in the range [100 - 200 m].

The selection of the earthquake that would produce the strongest ground shaking in the surrounding area, which is defined as the "controlling" earthquake (Kramer, 1996), was made by considering the Gutenberg-Richter relationship of the study area, the main active fault structure, and the empirical relationships which link the dimensions of the fault to the magnitude of the earthquakes, as described in detail in the section 4. Using a stress-drop value of 70 bar, the results in terms of the PGA, time histories and response spectra for the selected largest seismic event M_D = 4.3 are shown in Figures 9 and 10. A sensitivity analysis was carried out using different values of stress drop, those of 60, 70 and 80 bar, and the results of the simulations are summarized in Table 5 for all the study sites. The maximum values of A_{max}, obtained for a stress-drop value equal to 60, 70 and 80 bar, are in the ranges of, respectively [0.100-0.029] g, [0.120-0.033] g and [0.140-0.038] g.

The SM was also applied to the simulation of the ground motion for an M_D = 5.4 seismic event. Time histories and response spectra are shown in fig.11 and fig. 12 respectively. In this case we set the stress drop value equal to 70 bar. The maximum acceleration values obtained are in the range between 0.55 and 0.29 g for the high altitude sites (SGV, BAF, BKE, BKN, BKS, FTC) and between 0.32 and 0.17 g for the lower altitude sites (CDT, SVT, POL) where the urban density is higher (Table 6).

The standard deviations relative to the average maximum accelerations shown in table 5 and 6 are associated with the variability of stochastic component of the sub-source spectra and are of the order of 10% of the PGA value. The variability of ground motion associated with the uncertainty in the model parameters has been estimated to be as large as 35% of the ground motion parameters as observed by Sorensen et al. (2007). This result is in agreement with the variability of the ground motion associated with the simulation for M_D = 4.3 earthquake scenario, obtained for different values of stress drop (Table 5).

7. Discussion and conclusions

The stochastic finite-fault simulations reproduce reasonably well the ground motion for selected earthquakes ($1.7 \leq M_D \leq 3.6$). It is of note that the empirically defined strong-motion duration agrees with that estimated by theoretical considerations based on the assumption of a diffusive earth medium. This result allows this procedure to be exported to other volcanoes where there are not sufficient local earthquake recordings available to determine the empirical relationship between duration and distance. In synthesis, there is an important point to consider: it is necessary to precisely measure the average scattering properties of the seismic medium in order to bypass the lack of a sufficiently extended range of magnitudes and distances that are needed for a robust assessment of the correct empirical distance-duration relationships that characterize the volcanic area under study.

The stochastic procedure, validated on the observed waveforms, was used to simulate the synthetic waveforms for a possible future earthquake of $M_D \geq 4.3$. The earthquake that is expected to produce the strongest level of shaking was selected by considering G&R relationship and historical study on the past eruptions for the selected area. The corresponding magnitude, which we have indicated as M_{max}, was derived from the empirical relationship which relates the fault dimension to the magnitude of the "controlling" earthquake. On the basis of an acceptable assumption on size and source location, as explained in section 4, we selected the "controlling" earthquake M_D = 4.3. This is the maximum in a "statistical sense", as it is derived from the statistical distribution of the magnitude in the time interval between the early sixties and today. Implicit in this choice is the assumption that the tectonic regime associated with the volcanic

activity of Mt Vesuvius is stationary, and that the seismic catalogue used to estimate the Gutenberg-Richter relationship reflects this stationarity. The maximum acceleration values deduced by the synthetic waveforms for this event are in the range between 0.140 and 0.038 g. The values of A_{max} , obtained in this way for the M_D = 4.3, are similar to those calculated from ground motion predictive relationships for the reference hazard map of Italy (Montaldo et al., 2005). These authors evaluated maximum acceleration in hazard calculation for volcanic areas of Italian territory by RVT method for M_W = 4.5 and $\Delta\sigma$ = 50 bar scenario earthquake, values that are slightly different from those of the present paper. A direct comparison with our results is consequently impossible, but the acceleration values evaluated for M_D = 4.3 (table 5) are only slightly different for the investigated sites than the values calculated from regional attenuation for volcanic areas (Montaldo et al., 2005, fig.11). This small discrepancy (less than 30% of PGA values shown in table 5) can be due to the higher values of stress drop used here (60,70 and 80 bar), as well as to the different attenuation factor Q (Q = 250 in the work of Montaldo et al., 2005 and Q=150 in the present work) and to the site effect correction factor for the sites of interest applied in our work.

Higher values of A_{max} [A_{max} = 0.32 g (CDT) is the maximum acceleration value among the recording sites located in the urban area] were obtained by considering M_D = 5.4. An earthquake of this magnitude struck the Vesuvius area 17 years before the big Pompei eruption. It can reasonably be considered as the maximum that has ever occurred in this area in historical times. It appears quite evident that we have no chance to decide whether or not the "statistical" estimate of M_{max} is the most reasonable, because we have no idea of which tectonic regime might be associated with a renewal of volcanic activity of Mt Vesuvius. Therefore, we propose two alternatives: the first (M_{max} = 4.3) is based on the assumption of a substantial stationarity of the seismic regime, taken by extrapolating the present rate of seismicity, as the G&R predicts. The second alternative (M_D = 5.4) is in our opinion the worst possible scenario, which could happen in the case of a huge Plinian eruptions, as the Pompei eruption of 79 d.C. which occurred after a strong change in the local seismo-tectonic regime of the area.

Acknowledgments

We thank Francesca Bianco, Guido Ventura and Giuseppe Vilardo for the useful discussion and informations about attenuation, hypocentral locations, the geometrical features and the size of the fault system of Mt. Vesuvius. Nelson Pulido and an anonymous reviewer are gratefully acknowledged for their comments and suggestions which greatly improved the clarity of the paper. This work was partially funded by the Italian Dipartimento della Protezione Civile in the frame of the 2004-2006 Agreement with Istituto Nazionale di Geofisica e Vulcanologia – INGV, project V3_4.

References

Akinci, A., L. Malagnini, R. B. Herrmann, N. A. Pino, L. Scognamiglio, H. Eyidogan (2001). High-frequency Ground Motion in the Erzincan Region, Turkey: Inferences from Small Earthquakes, *Bull. Seism. Soc. Am.* **91**, n.6, 1446-1455.

Atkinson, G. M., D. Boore (1997). Stochastic point-source modelling of ground motions in the Cascadia Region. *Seism. Res. Let.* **68**, 74-85.

Atkinson, G. M., I.A. Beresenev (2002). Ground Motion at Memphis and St. Louis from M 7.5-8.0 Earthquakes in the New Madrid Seismic Zones, *Bull. Seism. Soc. Am.* **92**, 1015-1024.

Basham, P. W., D. H. Weichert, F. M. Anglin, M. J. Berry (1982). New probabilistic strong seismic ground motion maps of Canada: a compilation of earthquakes source zones, methods and results, *Earth Physics Branch Open-File Rept.* 82-33, 205 pp.

Benoit, J. P., S. R. Mc Nutt (1996). Global Volcanic earthquake swarms database and preliminary analysis of volcanic earthquake swarm duration, *Annali di Geofisica*, XXXIX, March 1996.

Berardi, R., M. J. Jiménez, G. Zonno, M. García-Fernández (2000). Calibration of stochastic finite-fault ground motion simulations for the 1997 Umbria-Marche, Central Italy, earthquake sequence, *Soil Dynamics and Earthquake Engineering*, **20**, 315-324.

Beresnev, I. A. and G. M. Atkinson (1997). Modeling finite-fault radiation from the ω2 spectrum, *Bull. Seism. Soc. Am.*, **87**, 67-84.

Beresnev, I. A. and G. M. Atkinson (1998a). FINSIM - a FORTRAN program for simulating stochastic acceleration time histories from finite fault, *Seism. Res. Lett.*, **69**, 27-52.

Beresnev, I. A. and G. M. Atkinson (1998b). Stochastic finite-fault modeling of ground motions from the 1994 Northridge, California, earthquake. I. Validation on rock sites, *Bull. Seism. Soc. Am.*, **88**, 1392-1401.

Bianco, F., M. Castellano, G. Milano, G. Ventura, G. Vilardo (1998). The Somma-Vesuvius stress-field induced by regional tectonic: evidences from seismological and mesostructural data, *J. Volcanol. Geotherm. Res.,* **82**, 199-218.

Bolt, B.A. (1969). Duration of strong motion, *Proceedings of the 4th World Conference on Earthquake Engineering*, Santiago, Chile, 1304-1315.

Boore, D.M. (2003). Simulation of ground motion using the stochastic method, *Pure Appl. Geophys.*, **160**, 635-676.

Boore, D.M. (1983). Stochastic simulation of high-frequency ground motions based on seismological model of the radiated spectra, *Bull. Seism. Soc. Am.*, **73**, 1865-1894.

Carvalho, A., M. L. Sousa, A. Campos Costa, J. C. Nunes, V. H. Forjaz (2001). Seismic hazard for the Central Group of the Azores Islands, *Bolletino di Geofisica Teorica ed Applicata*, **42**, No. 1-2, 89-105.

Carvalho, A., G. Zonno, G. Franceschina, J. Serra Bilè, A. Campos Costa (2007). Earthquake shaking scenarios for the mertropolitan area of Lisbon, *Soil Dynamics and Earthquake Engineering*, in press (doi:10.1016/j.soildyn.2007.07.009).

Castro, R.R., A. Rovelli, M. Cocco, M. Di Bona, F. Pacor (2001). Stochastic Simulation of Strong-Motion Records from the 26 September 1997 (Mw 6), Umbria-Marche (Central Italy) Earthquake, *Bull. Seismol. Soc. Am*., **91**, No.1, 27–39.

Castro, R.R., G. Franceschina, F. Pacor, D. Bindi, L. Luzi (2006). Analysis of the frequency dependance of the S-wave radiation pattern from local earthquakes in Central Italy, *Bull. Seismol. Soc. Am*., **96**, 415–426.

Castro, R.R., F. Pacor, G. Franceschina, D. Bindi, G. Zonno, L. Luzi (2007). Stochastic strong-motion simulation of the Umbria-Marche earthquake of September 1997 (M_W 6): comparison of different approaches, *Bull. Seismol. Soc. Am.*, in press.

Cubellis, E., G. Luongo, A. Maturano (2007). Seismic hazard assesment at Mt. Vesuvius: Maximum expected magnitude, *Journal of Volcanology and Geothermal Research,* **162**, 139-148.

Del Pezzo, E., F. Bianco, G. Saccorotti (2004). Seismic source dynamics at Vesuvius volcano, Italy, *Journal of Volcanology and Geothermal Research,* **133**, 23-49.

Del Pezzo, E., F. Bianco, L. Zaccarelli (2006a). Separation of Qi and Qs from passive data at Mt. Vesuvius: A reappraisal of the seismic attenuation estimates, *Physics of the Earth and Planetary Interiors*, **159**, 202-212.

Del Pezzo, E., F. Bianco, L. De Siena, A. Zollo (2006b). Small scale shallow attenuation structure at Mt. Vesuvius, Italy, *Physics of the Earth and Planetary Interiors,* **157**, 257-268.

Feheler, M. and H. Sato (2003). Coda, *Pure and Applied Geophysics*, **160**, Num. 3-4.

Festa, G., A. Zollo, G. Manfredi, M. Polese, E. Cosenza (2004). Simulation of Earthquake Ground Motion and effects on engineering Structures during the Preeruptive Phase of an Active Volcano, *Bull. Seismol. Soc. Am*., **94**, No.6, 2213-2221.

Galluzzo, D., E. Del Pezzo, M. La Rocca, S. Petrosino (2004). Peak Ground Acceleration produced by local earthquakes in volcanic areas of Campi Flegrei and Mt. Vesuvius, *Annals of Geophysics*, **47**, n. 4.

Galluzzo, D., E. Del Pezzo, R. Maresca, M. La Rocca, M. Castellano (2006). Site-effect estimation and source-scaling dynamics for local earthquakes at Mt. Vesuvius, Italy, *Proceedings at Third International Symposium of Surface Geology on Seismic Motion*; Grenoble, France, September 2006.

Gusev, A. A. (1983). Descriptive statistical Model of Earthquake Source radiation and its Application to an Estimation of Short-Period Strong Motion, *Geophys. J. R. astr. Soc.*, **74**, 787-808.

Kagan, Y. Y. (1997). Seismic moment-frequency relation for shallow earthquakes: Regional Comparison, *J. Geophys. Res.*, **102** (B2), 2835-2852.

Kawashima, K., K. Aizawa, K. Tahahashi (1985). Duration of strong motion acceleration records, *Proc. of JSCE Structural Eng./Earthquake Eng.* (1985) 2, 2.

Kramer, S. (1996). *Geotechnical Earthquake Engineering*, Prentice Hall International Series.

Lay, T. and Wallace T. C. (1995). *Modern Global Seismology*, Academic Press.

Montaldo, V., E. Faccioli, G. Zonno, A. Akinci, L. Malagnini (2005). Treatment of ground motion predictive relationships for the reference seismic hazard map of Italy, *Journal of Seismology*, **9**, 295-316.

Motazedian, D.and G. M. Atkinson (2005a). Earthquake Magnitude Measurements for Puerto Rico, *Bull. Seismol. Soc. Am.*, **95**, 725–730.

Motazedian, D.and G. M. Atkinson (2005b). Stochastic finite-fault modelling based on a dynamic corner frequency, *Bull. Seismol. Soc. Am.*, **95**, 995–1010.

Petukhin, A. G. and A. A. Gusev (2003). The Duration-distance relationship and Average Envelope Shapes of Small Kamchatka Earthquakes, *Pure and Applied Geophysics*, **160**, 1717-1743.

Pousse G., L. F. Bonilla, F. Cotton, L. Margerin (2006). Nonstationary Stochastic Simulation of Srong Ground Motion Time Histories Including Natural Variability :Application to the K-Net Japanese Database, *Bull. Seism. Soc. Am.*, **96**, 2103-2117.

Pulido N. and Kubo T. (2004). Near-fault strong motion complexity of the 2000 Tottori earthquake (Japan) from a broadband source asperity model, *Tectonophysics*, **390**, 177-192.

Rayleigh, J. W. S. (1945). *The Theory of Sound*, MacMillan, New York, 1896 (Reprinted by Dover, New York, vol.2, 1945).

Sabetta F. and A. Pugliese (1996). Estimation of response spectra and simulation of nonstationary earthquake ground motions, *Bull. Seism. Soc. Am.*, **86**, 337-352.

Sato, H. and M. Fehler (1997). *Seismic Wave Propagation and Scattering in the heterogenous Earth*, Springer-Verlag New York.

Scarpa R., F. Tronca, F. Bianco, E. Del Pezzo (2002). High resolution velocità structure beneath Mt Vesuvius from seismic array data, *Geophys. Res. Lett.*, **29** (21), 2040-2044.

Sorensen, M.B., N. Pulido, K. Atakan (2007). Sensitivity of Ground-Motion Simulations to Earthquake Source Parameters: A Case Study for Istambul, Turkey, *Bull. Seism. Soc. Am.*, **97**, 881-900.

Trifunac M. D. and A. G. Brady (1975). A study on the duration of strong earthquake ground motion, *Bull. Seism. Soc. Am.*, **65**, 581-626.

Varadan V. K., V. V. Varadan, Y. H. Pao (1978). Multiple Scattering of Elastic Waves by cylinders of arbitrary cross-section, I. SH waves, *J. Acoustic Soc. Am.*, **63**, 1310-1319.

Wells D. L. and K. J. Coppersmith (1994). New empirical relationships among magnitude, rupture

length, rupture width, rupture area and surface displacement, *Bull. Seism. Soc. Am.*, **84**,974-1002.

Zollo A., W. Marzocchi, P. Capuano, A. Lomax, G. Iannaccone (2002). Space and time behaviour of seismic activity at Mt. Vesuvius volcano, Southern Italy, *Bull. Seismol. Soc. Am.*, **92**, 625-640.

Istituto Nazionale di Geofisica e Vulcanologia
Sezione di Napoli "Osservatorio Vesuviano"
Via Diocleziano, 328
80124 NAPOLI, Italy
galluzzo@ov.ingv.it
delpezzo@ov.ingv.it
(D.G.,E.D.P.)

Istituto Nazionale di Geofisica e Vulcanologia
Sezione di Milano-Pavia
Via Bassini, 15
20133 MILANO, Italy
zonno@mi.ingv.it
(G.Z.)

Appendix

Recent efforts have been made to quantitatively describe strong-motion duration in terms of earthquake magnitude, source-to-station distance and effect of geological environment (Williamson, 1972). The general observation is that a seismic wave packet broadens as a function of distance and of the heterogeneity of the seismic medium. The knowledge of the earth medium properties of the Mt Vesuvius area has been refined recently using transport theory and by interpreting the seismic coda energy envelope as generated by a diffusion process (Del Pezzo et al., 2006). In diffusive environments, the scattering properties can significantly affect the duration of the seismic ground motion (Petukhin and Gusev, 2003). In the present study, we have evaluated the time duration for the selected seismograms using the definition of Gusev (1983; T_{rms}) as given by Petukhin and Gusev (2003) and calculated the theoretical duration as a function of the intrinsic dissipation and scattering coefficient (Fehler and Sato, 2003). The T_{rms} duration is defined through the normalized second central moment of the squared signal $A(t)^2$ by considering the following relationship (Gusev, 1983):

$$T_{RMS}^2 = e_2 / e_0 - (e_1 / e_0)^2 \tag{3}$$

where e_j are j-th power moments over time, defined as:

$$e_j = \int_0^{+\infty} t^j \cdot A^2(t) dt \quad (j = 0,1,2) \tag{4}$$

The full seismogram envelope is well described by transport theory, which is also known as radiative transfer theory, and which has been well known for many years in many fields of physics, including acoustics and optics (Rayleigh, 1945; Varadan et al., 1978). The application of this theory to the energy envelopes of the seismograms recorded at Mt Vesuvius has revealed that the propagation of the high frequency wavefield takes place in a diffusive regime (Del Pezzo et al., 2006). The same authors calculated the diffusivity and the intrinsic dissipation parameters that characterize the Mt Vesuvius zone.

Assuming a diffusive regime, we can use the equation describing the lapse-time dependence of the seismic energy envelope as a function of energy at source and distance (Sato and Fehler, 1997), and apply the definition of duration given by Gusev (1983) to this envelope. In this way, we obtain a theoretically based set of distance duration curves at given magnitudes, which depend on the diffusivity and intrinsic dissipation measured (independently) in the area under study.

The diffusion equation can be written as:

$$E_D\left(r,f,t,E_0,v,Q_I^{-1},Q_S^{-1}\right)=\frac{E_0}{\left(4\pi Dt\right)^{3/2}}\cdot K\left(\frac{vt}{r}\right)\cdot H\left(t\right)\cdot \mathrm{e}^{\left(-Q_I^{-1}2\pi ft-\left(r^2/4Dt\right)\right)} \quad (5)$$

where E_D is the energy flux density, f is the frequency, Q_S is the scattering quality factor, v is the wave speed, Q_I is the intrinsic quality factor, r is the source station distance, E_0 is the energy at source, t is the lapse time, H(t) is the Heaviside step function, and D is the diffusivity, which is given by:

$$D=\frac{v^2}{6\pi\ f\ Q_S^{-1}} \quad (6)$$

The analytical form of the K(x) function is given by (Sato and Fehler, 1998):

$$K(x)=(1/x)\ln[(x+1)/(x-1)] \quad (7)$$

The energy flux density described by equation (5) represents the energy envelope for the seismogram filtered at central frequency f; in our application, the evaluation of the strong-motion duration T_{RMS} was made on the energy flux density evaluated across the whole range of investigated frequencies, as:

$$E_{DENV}\left(r,t,E_0,v,Q_I^{-1},Q_S^{-1}\right)=\sum_f E_D\left(r,f,t,E_0,v,Q_I^{-1},Q_S^{-1}\right) \quad (8)$$

The results show a good agreement between the time durations evaluated from the observed waveform (Fig. 3, grey filled squares) and the theoretical diffusion model obtained for the BKE, BAF, SGV and FTC stations (Fig. 3, open circles).

Scenario Earthquake Fault Parameters		
M_{max}	$M_D = 4.3$	$M_D = 5.4$
Dimension	2.0 x 2.0 km^2	4.0 x 8.0 km^2
Hypocenter	Latitude = 40° 49’ 52’’ N	Latitude = 40° 49’ 52’’ N
	Longitude = 14° 25’ 52’’ E	Longitude = 14° 25’ 52’’ E
	Depth = 4.0 km b.s.l	Depth = 4.0 km b.s.l
Dip Angle	60°	60°
Strike Angle	135°	135°

Table 1

Date (yy-mm-dd-hh-mm)	Lat. (N)	Long. (E)	Depth (km)	M_D	Strike (°)	Dip (°)
99-07-03-22-51	40° 49’ 26’’	14° 25’ 12’’	1.7	1.7	265°	55°
99-08-05-21-17	40° 49’ 33’’	14° 25’ 22’’	1.7	1.9	245°	60°
99-03-11-03-49	40° 49’ 25’’	14° 25’ 39’’	2.6	2.0	185°	30°
99-09-30-08-22	40° 49’ 26’’	14° 25’ 36’’	2.0	2.1	100°	80°
99-04-12-11-07	40° 49’ 24’’	14° 25’ 39’’	1.4	2.4	195°	40°
99-10-11-05-05	40° 49’ 28’’	14° 25’ 39’’	1.5	2.6	165°	70°
99-11-05-05-55	40° 49’ 26’’	14° 25’ 31’’	1.5	2.7	255°	75°
99-11-10-20-14	40° 49’ 49’’	14° 25’ 46’’	1.7	2.8	170°	85°
99-10-11-04-35	40° 49’ 29’’	14° 25’ 34’’	1.6	3.3	65°	5°
99-10-09-07-41	40° 49’ 52’’	14° 25’ 52’’	4.0	3.6	170°	85°

Table 2

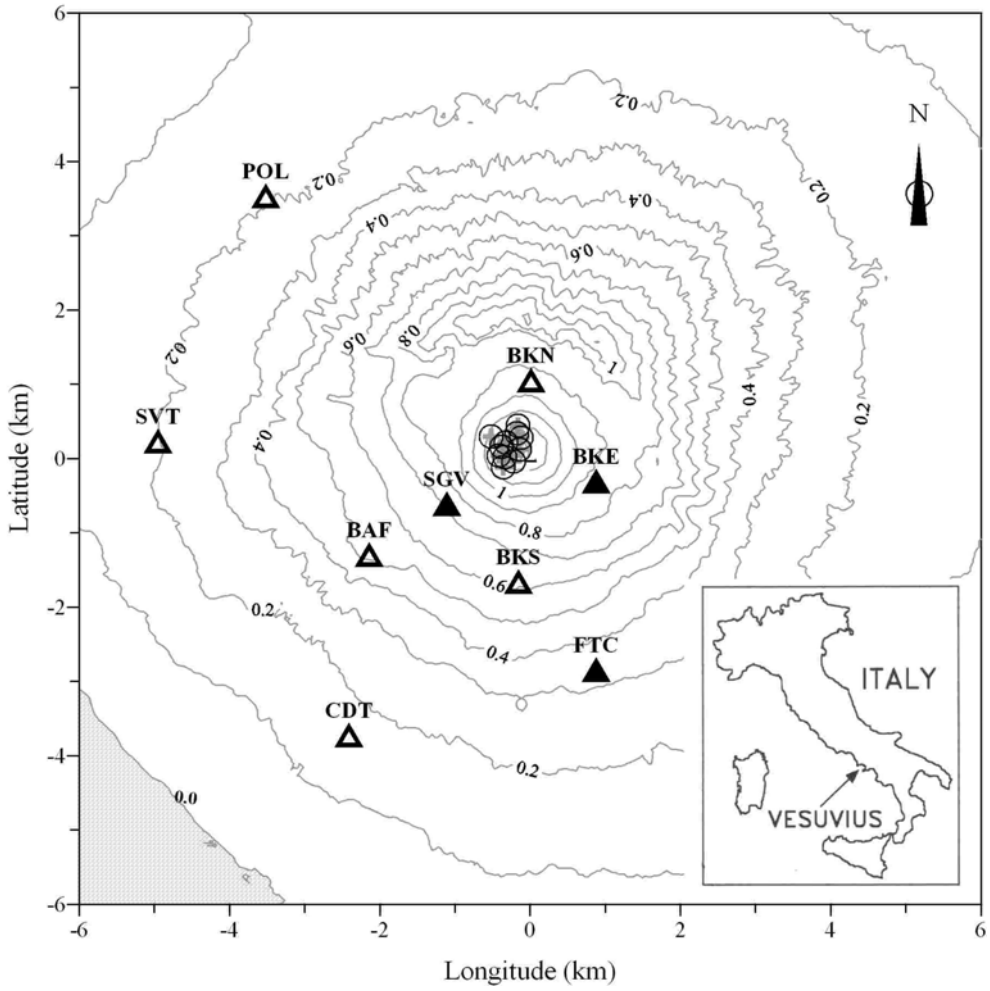
N
POL
SVT
BKN
BKE
SGV
BAF
BKS
FTC
CDT
ITALY
VESUVIUS
Latitude (km)
Longitude (km)
6
4
2
0
-2
-4
-6
0.2
0.4
0.6
0.8
1
0.0

Figure 1

Model Parameters	Value	Reference
Fault dimension	Table 1	Wells and Coppersmith, 1994
Average shear wave velocity	2.0 km/s	Scarpa et al., 2002
Average attenuation parameter	Q =150	Del Pezzo et al., 2006
Density	ρ=2.5 g/cm^3	Zollo et al., 2002
Site effect empirical functions	See fig.6	Galluzzo et al., 2006
f_{max}	20 Hz	-
Ground motion duration	T_{rms} = 6.1s	Gusev, 1983

Table 3

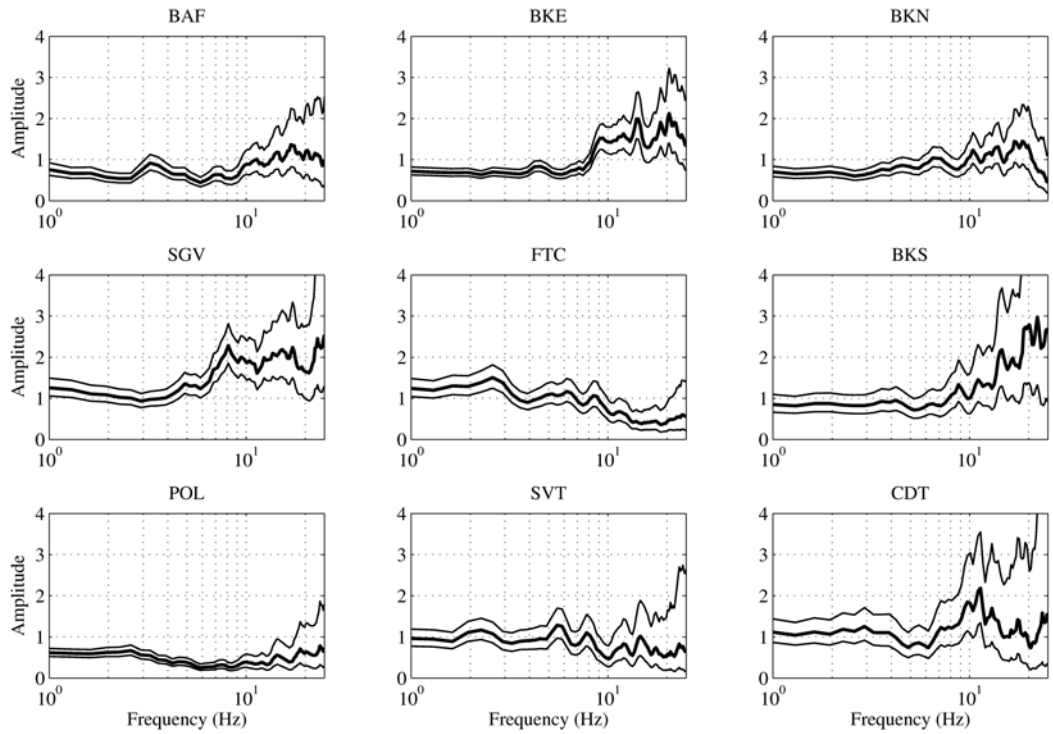

Figure 2

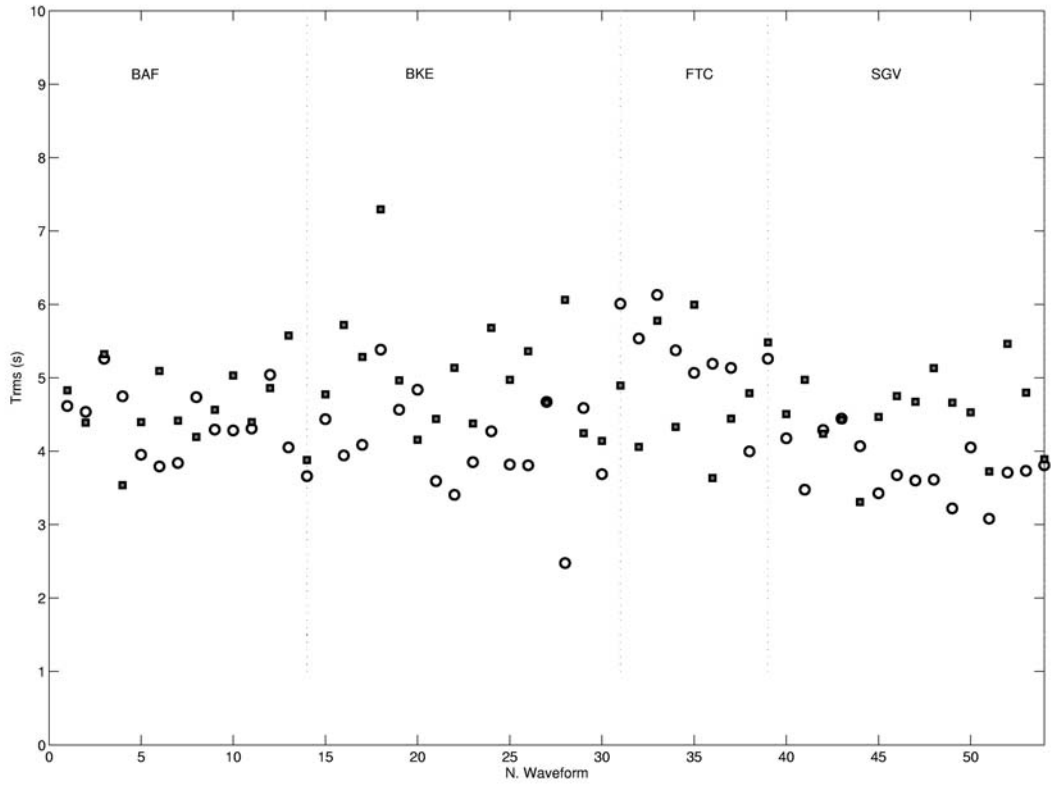
BAF
BKE
FTC
SGV
Trms (s)
N. Waveform
0
1
2
3
4
5
6
7
8
9
10
0
5
10
15
20
25
30
35
40
45
50

Figure 3

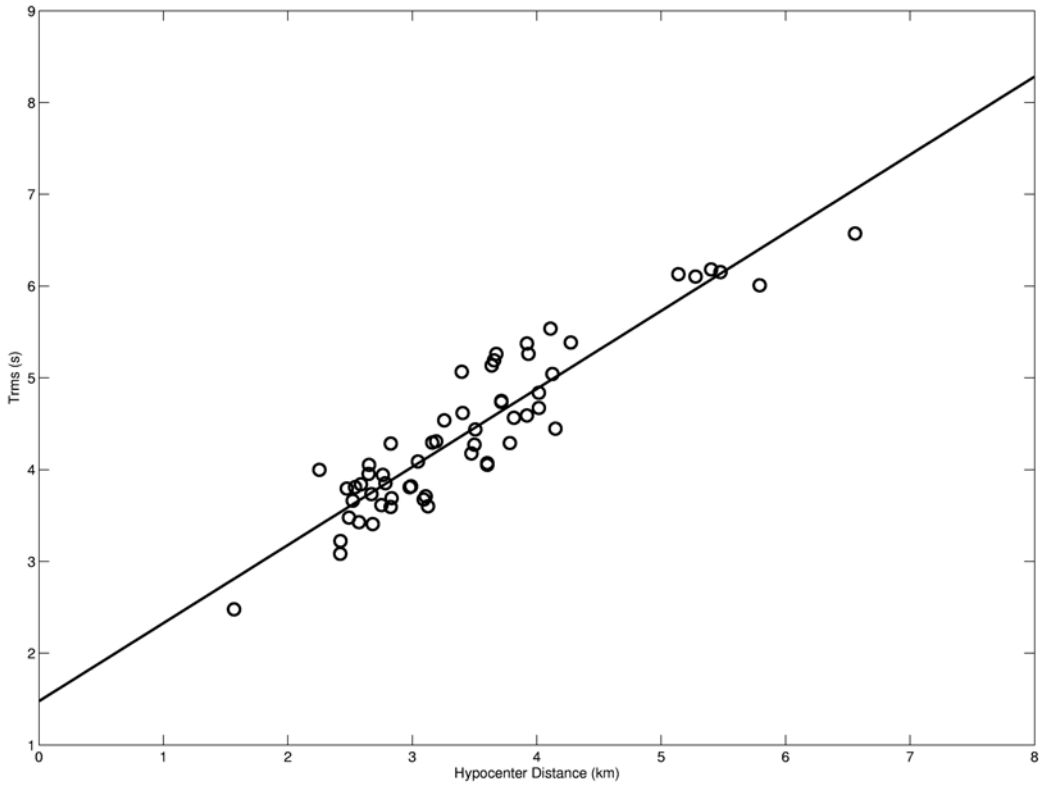

Figure 4

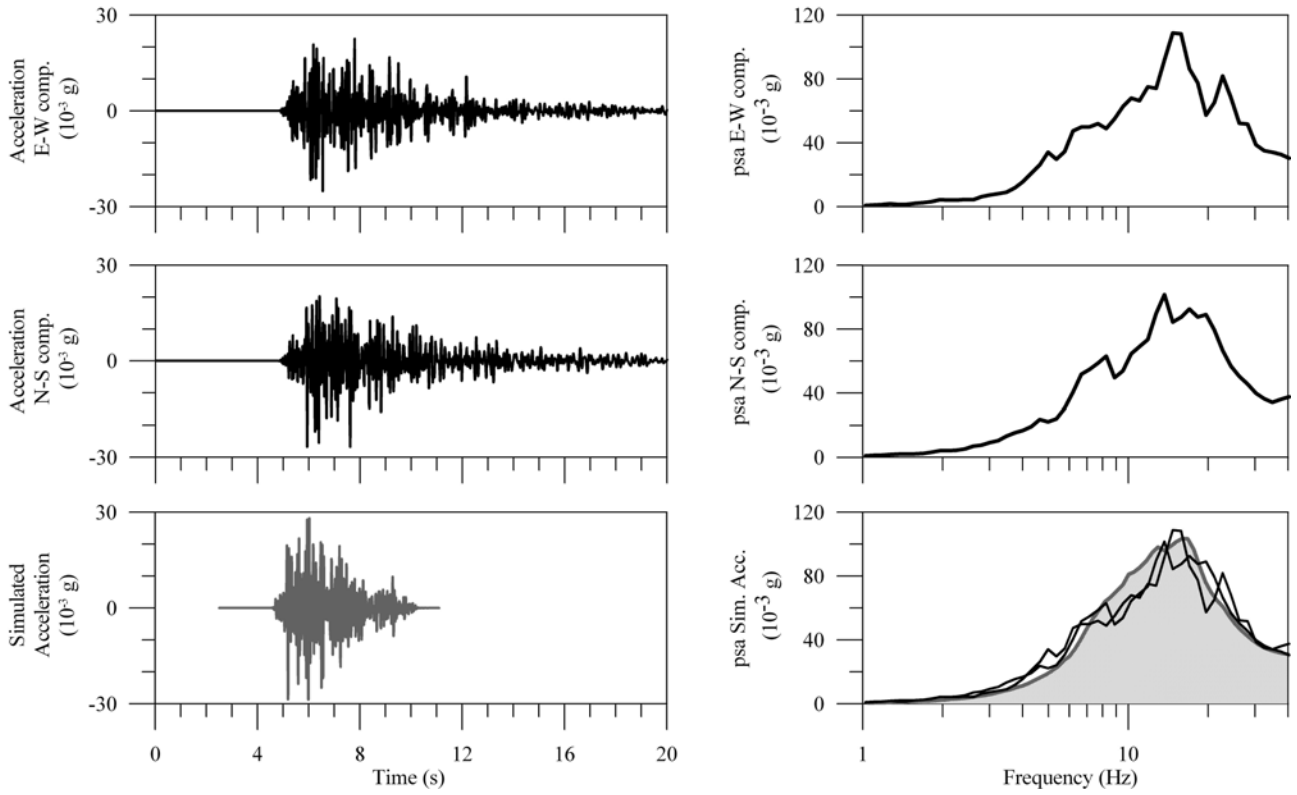
Acceleration E-W comp. (10^{-3} g)
Acceleration N-S comp. (10^{-3} g)
Simulated Acceleration (10^{-3} g)
30
0
-30
0
4
8
12
16
20
Time (s)
psa E-W comp. (10^{-3} g)
psa N-S comp. (10^{-3} g)
psa Sim. Acc. (10^{-3} g)
120
80
40
0
1
10
Frequency (Hz)

Figure 5

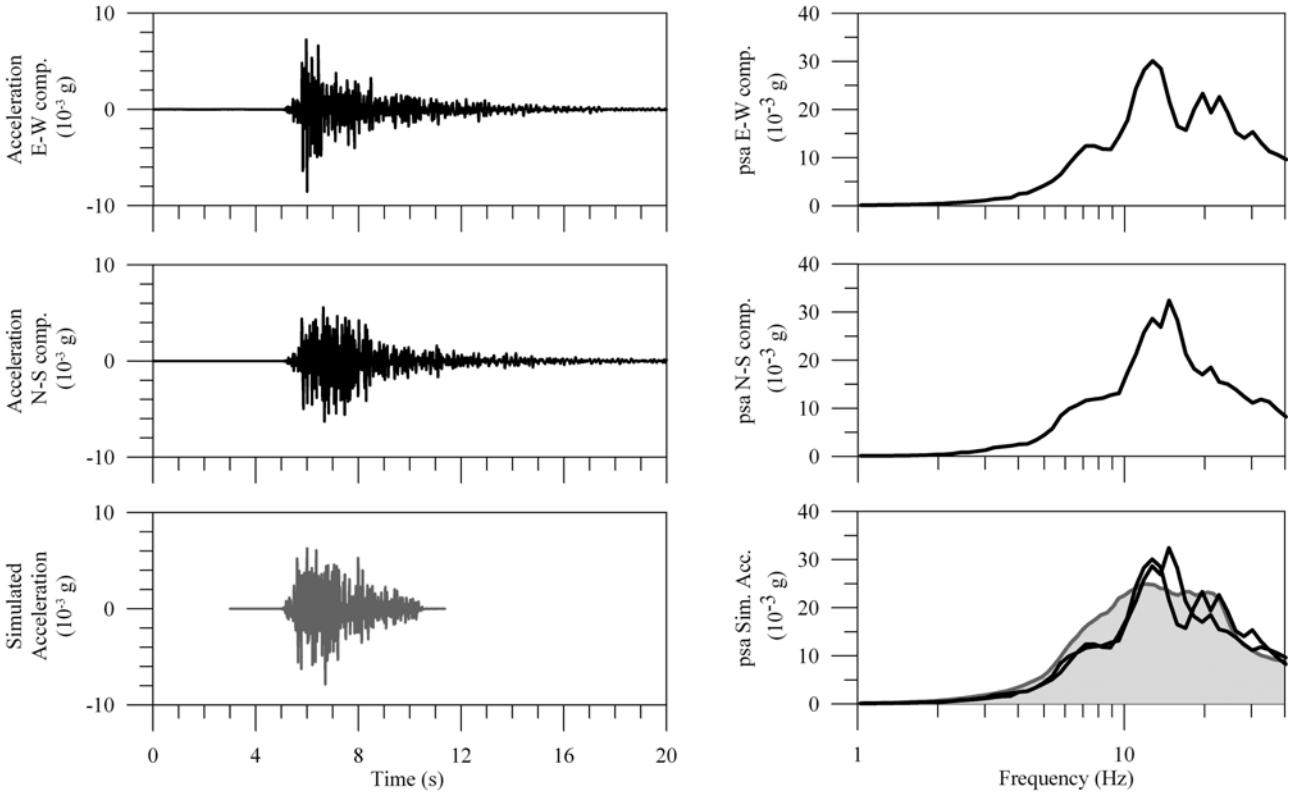
Acceleration E-W comp. (10^{-3} g)
Acceleration N-S comp. (10^{-3} g)
Simulated Acceleration (10^{-3} g)
Time (s)
psa E-W comp. (10^{-3} g)
psa N-S comp. (10^{-3} g)
psa Sim. Acc. (10^{-3} g)
Frequency (Hz)

Figure 6

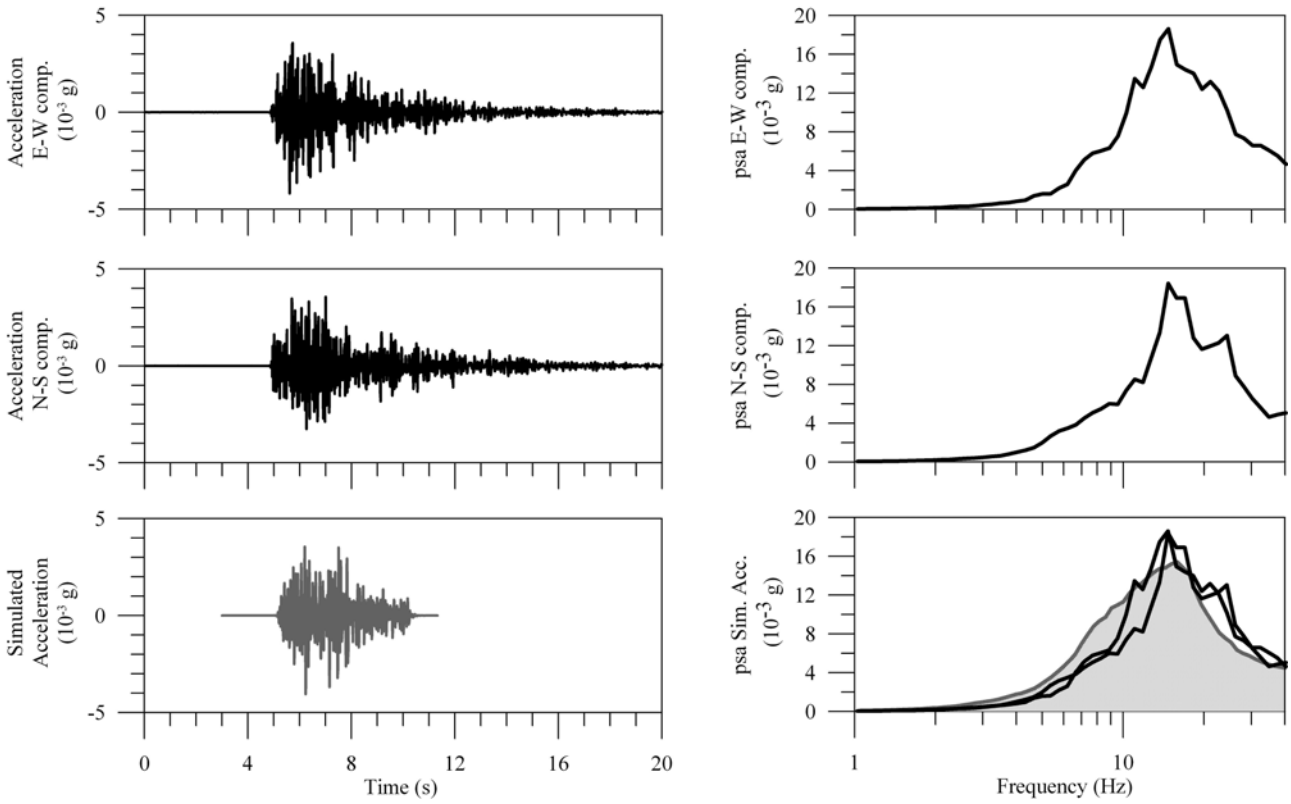
Acceleration E-W comp. (10^{-3} g)
Acceleration N-S comp. (10^{-3} g)
Simulated Acceleration (10^{-3} g)
Time (s)
psa E-W comp. (10^{-3} g)
psa N-S comp. (10^{-3} g)
psa Sim. Acc. (10^{-3} g)
Frequency (Hz)

Figure 7

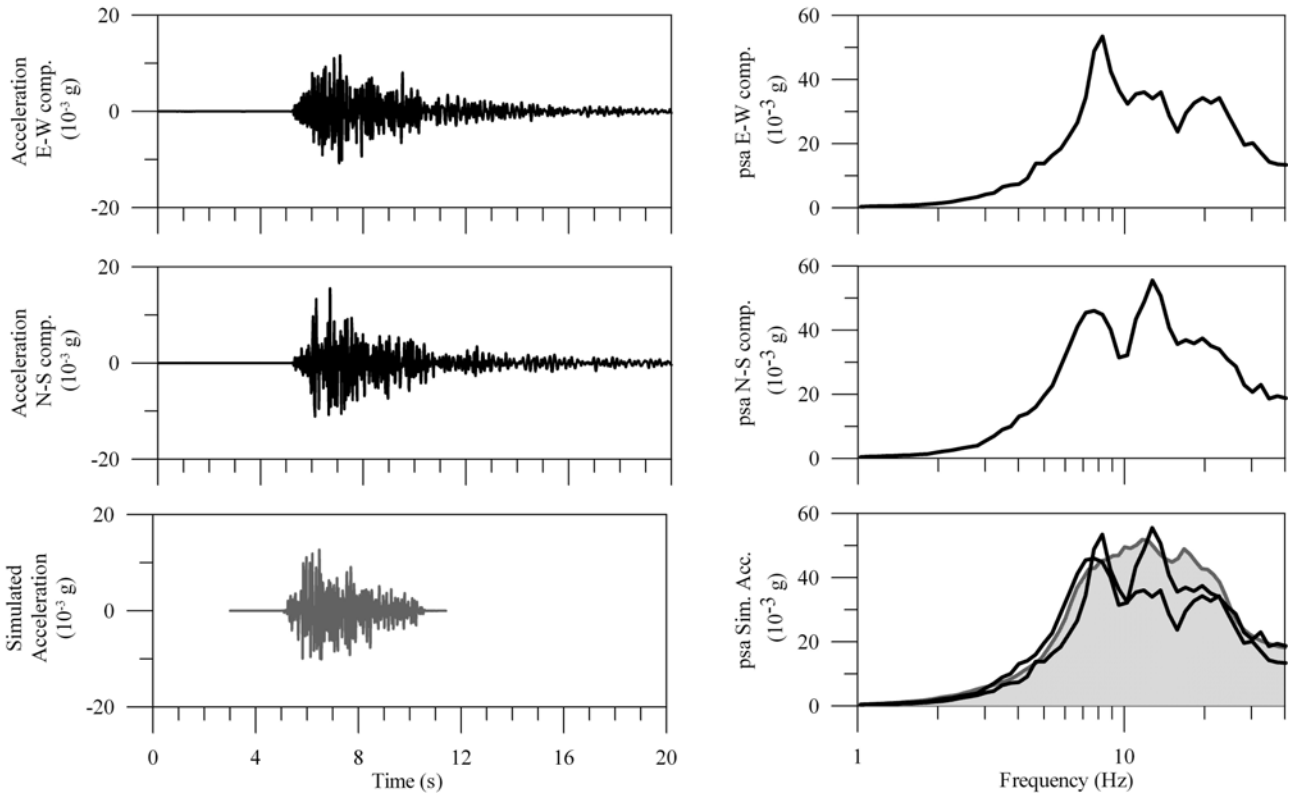
Acceleration E-W comp. (10^{-3} g)
Acceleration N-S comp. (10^{-3} g)
Simulated Acceleration (10^{-3} g)
20
0
-20
0
4
8
12
16
20
Time (s)
psa E-W comp. (10^{-3} g)
psa N-S comp. (10^{-3} g)
psa Sim. Acc. (10^{-3} g)
60
40
20
0
1
10
Frequency (Hz)

Figure 8

Date (yy-mm-dd-hh-mm)	M_D	L x W (km^2)	$\Delta\sigma$ (bar)	D (s)	|Obs. A_{max}| (10^{-3} g)	|Simul. A_{max}| ; σ (10^{-3} g)
99-07-03-22-51	1.7	0.18 x 0.18	6	4.3	1.3	1.2 ; 0.1
99-08-05-21-17	1.9	0.23 x 0.23	6	4.2	2.0	2.0 ; 0.3
99-03-11-03-49	2.0	0.25 x 0.25	5	4.8	0.7	0.8 ; 0.1
99-09-30-08-22	2.1	0.30 x 0.30	5	4.3	0.5	0.6 ; 0.1
99-04-12-11-07	2.4	0.35 x 0.42	6	3.8	3.6	4.0 ; 0.6
99-10-11-05-05	2.6	0.42 x 0.42	6	3.9	4.1	4.2 ; 0.6
99-11-05-05-55	2.7	0.45 x 0.45	6	4.0	3.7	3.7 ; 0.5
99-11-10-20-14	2.8	0.50 x 0.50	5	4.2	3.7	4.2 ; 0.8
99-10-11-04-35	3.3	0.80 x 0.80	9	4.0	16.0	17.0 ; 3.0
99-10-09-07-41	3.6	1.00 x 1.20	50	6.1	28.0	29.0 ; 5.0

Table 4

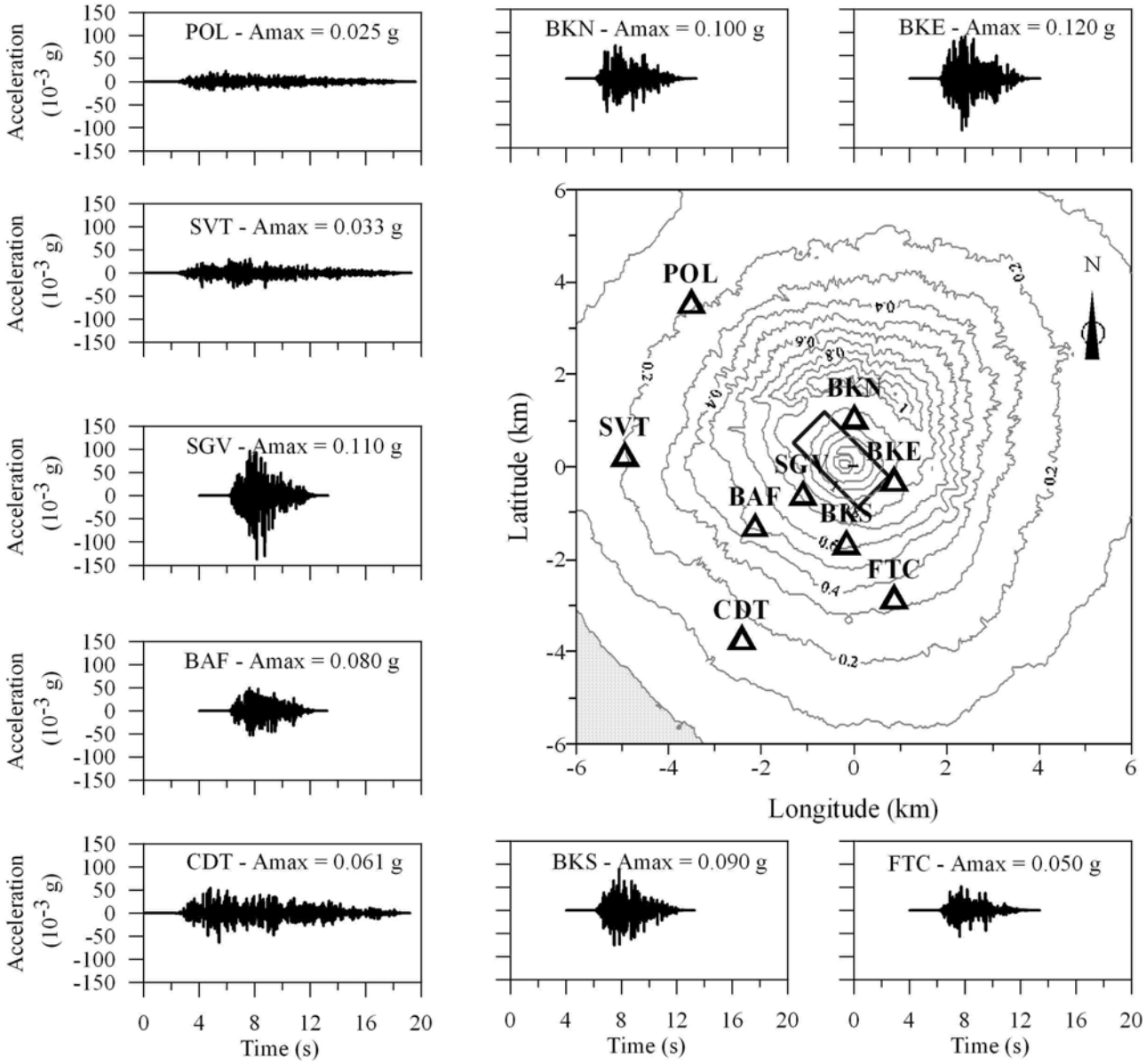
POL - Amax = 0.025 g
BKN - Amax = 0.100 g
BKE - Amax = 0.120 g
SVT - Amax = 0.033 g
SGV - Amax = 0.110 g
BAF - Amax = 0.080 g
CDT - Amax = 0.061 g
BKS - Amax = 0.090 g
FTC - Amax = 0.050 g
Acceleration (10^-3 g)
Time (s)
Latitude (km)
Longitude (km)
N
POL
SVT
BKN
SGV
BKE
BAF
BKS
FTC
CDT

Figure 9

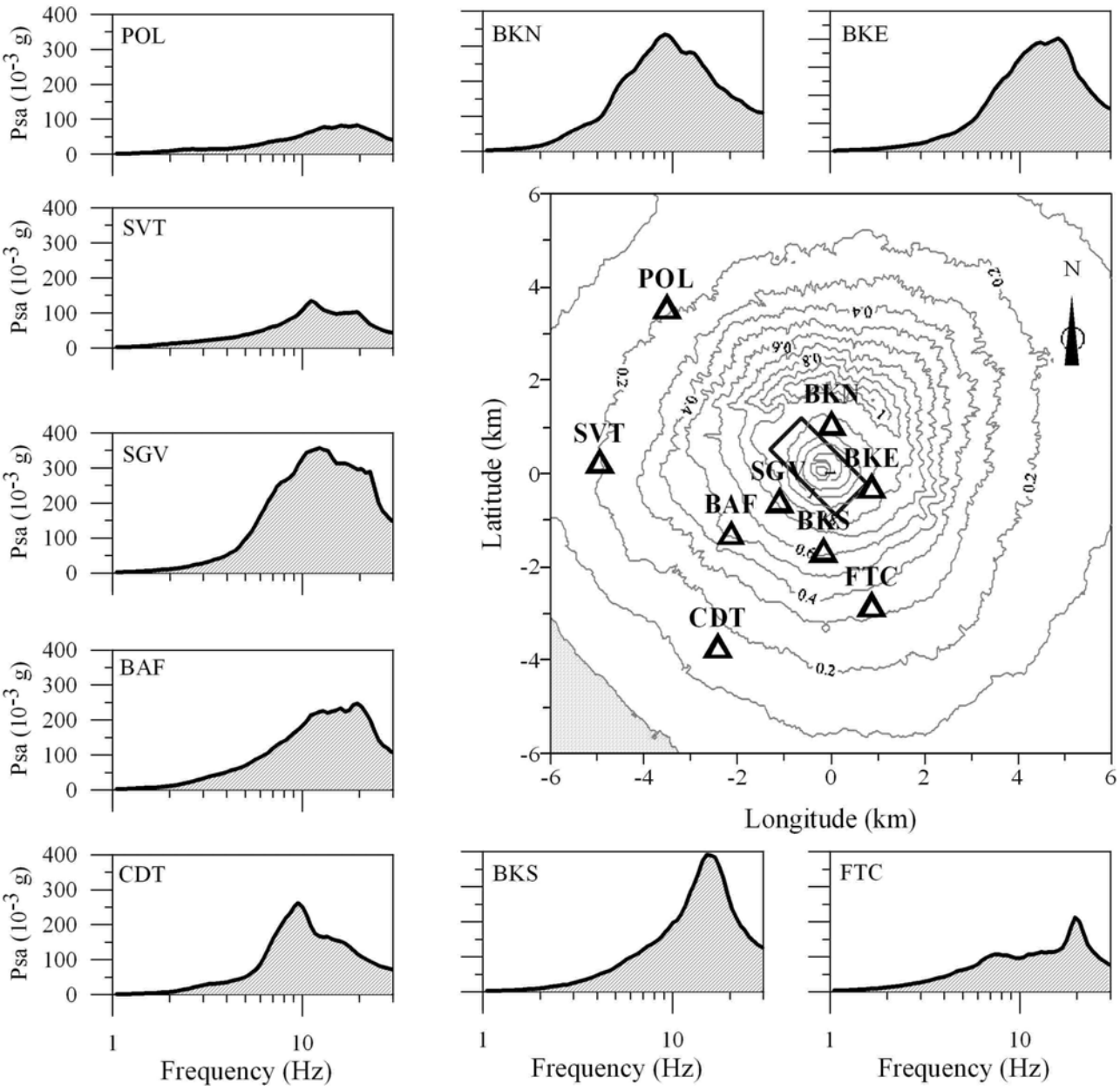
POL
BKN
BKE
SVT
SGV
BAF
CDT
BKS
FTC
Psa (10-3 g)
Frequency (Hz)
Latitude (km)
Longitude (km)
N

Figure 10

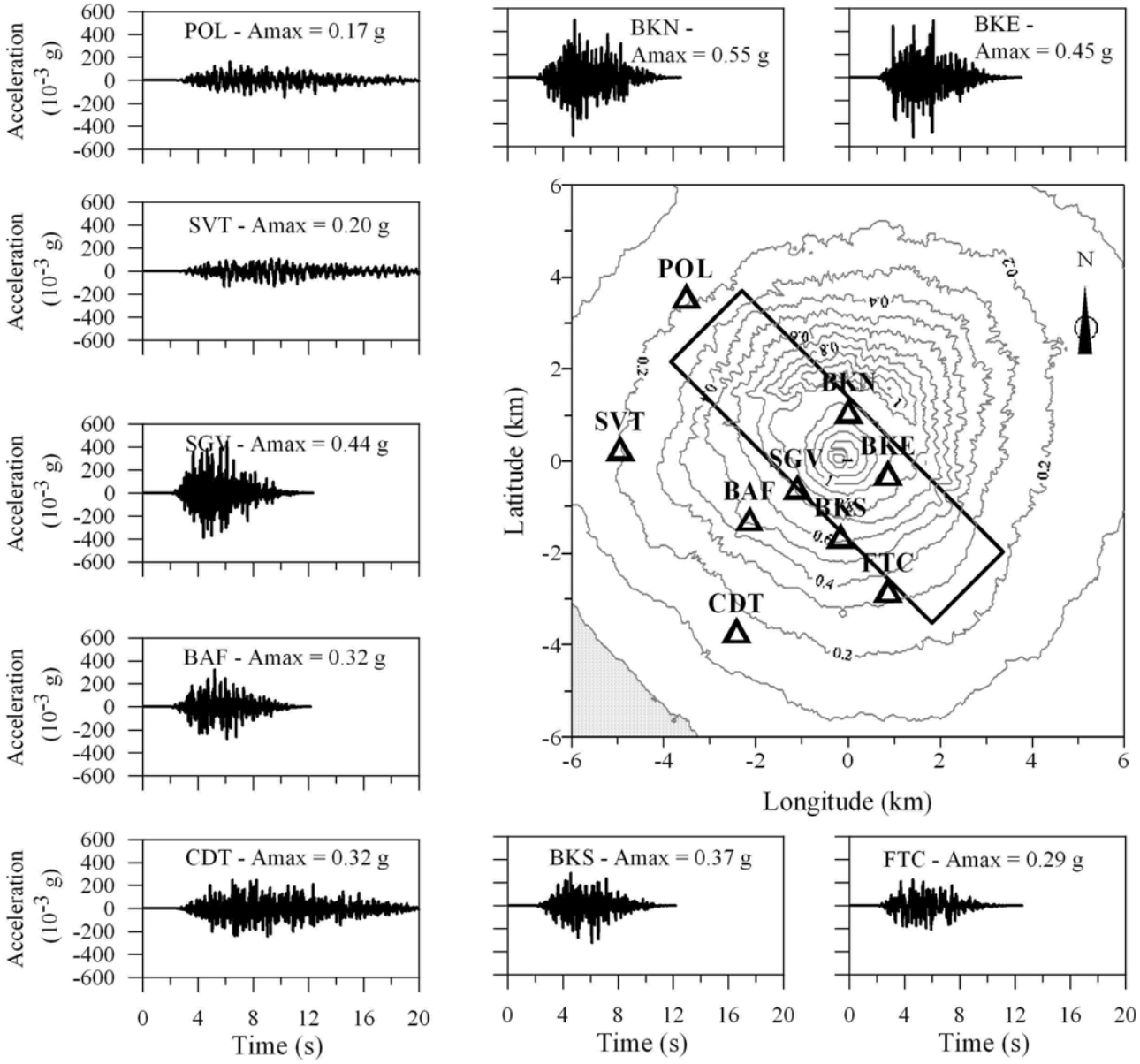
POL - Amax = 0.17 g
BKN - Amax = 0.55 g
BKE - Amax = 0.45 g
SVT - Amax = 0.20 g
SGV - Amax = 0.44 g
BAF - Amax = 0.32 g
CDT - Amax = 0.32 g
BKS - Amax = 0.37 g
FTC - Amax = 0.29 g
Acceleration (10^-3 g)
Time (s)
Latitude (km)
Longitude (km)
N
POL
SVT
BKN
BKE
SGV
BAF
BKS
FTC
CDT

Figure 11

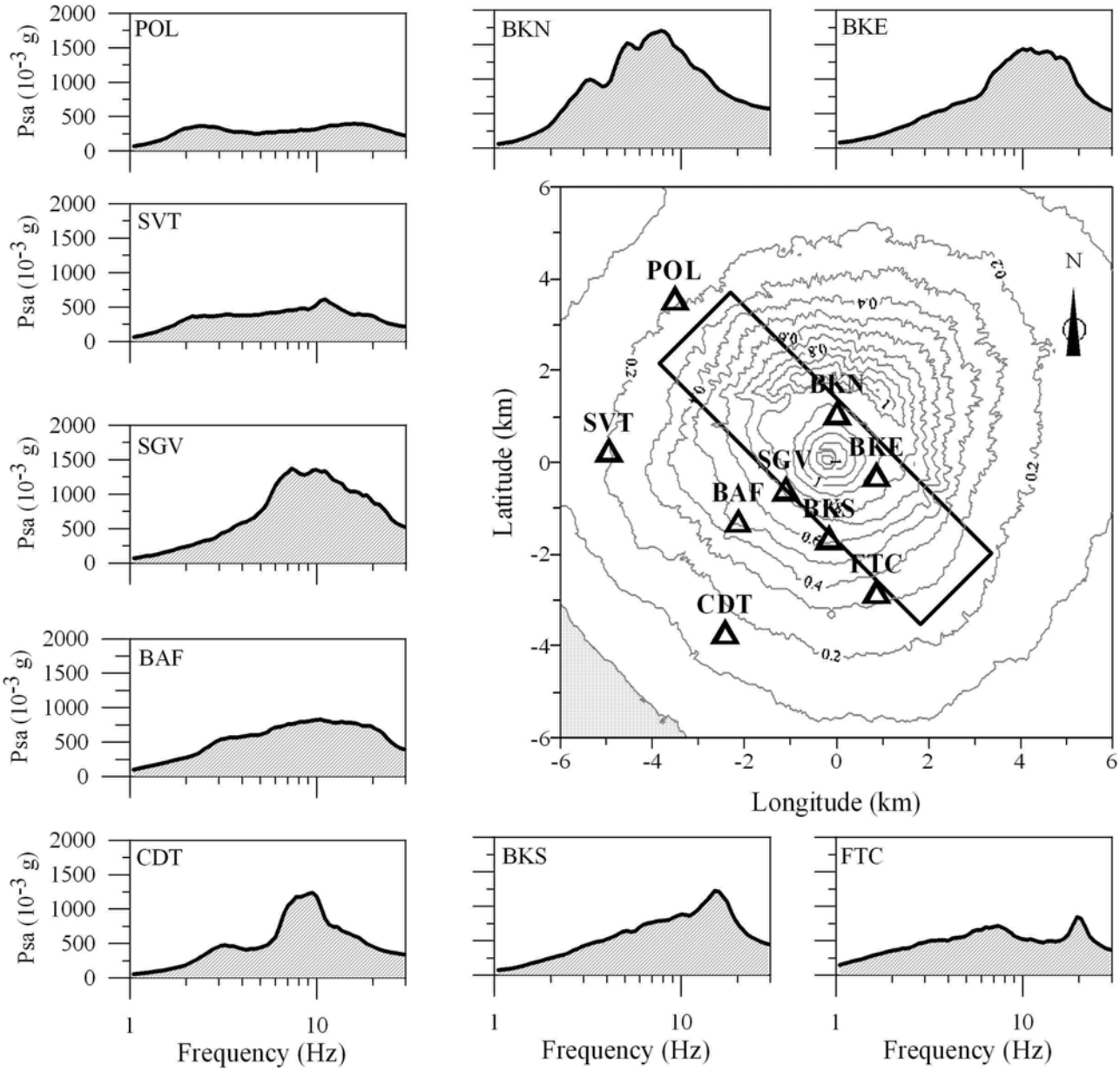
POL
BKN
BKE
SVT
SGV
BAF
BKS
FTC
CDT
Psa (10-3 g)
Frequency (Hz)
Latitude (km)
Longitude (km)
N

Figure 12

Station-Site	A_{max} (g) ; σ A_{max} (g) ($\Delta\sigma$ = 60 bar)	A_{max} (g) ; σ A_{max} (g) ($\Delta\sigma$ = 70 bar)	A_{max} (g) ; σ A_{max} (g) ($\Delta\sigma$ = 80 bar)
BAF	0.070 ; 0.010	0.080 ; 0.010	0.090 ; 0.010
BKE	0.100 ; 0.020	0.120 ; 0.020	0.140 ; 0.030
BKN	0.080 ; 0.010	0.100 ; 0.010	0.110 ; 0.020
SGV	0.090 ; 0.010	0.110 ; 0.010	0.130 ; 0.010
FTC	0.040 ; 0.010	0.050 ; 0.010	0.060 ; 0.010
BKS	0.080 ; 0.010	0.090 ; 0.020	0.110 ; 0.020
POL	0.021 ; 0.002	0.025 ; 0.002	0.028 ; 0.002
SVT	0.029 ; 0.003	0.033 ; 0.003	0.038 ; 0.004
CDT	0.053 ; 0.006	0.061 ; 0.007	0.070 ; 0.008

Table 5

Station-Site	A_{max} (g) ; σ A_{max} (g) ($\Delta\sigma$ = 70 bar)
BAF	0.32 ; 0.04
BKE	0.45 ; 0.06
BKN	0.55 ; 0.07
SGV	0.44 ; 0.05
FTC	0.29 ; 0.04
BKS	0.37 ; 0.06
POL	0.17 ; 0.02
SVT	0.20 ; 0.03
CDT	0.32 ; 0.04

Table 6

Figure captions

Figure 1. Epicenters of selected local earthquakes (open black circles filled with grey cruises) in the Mt Vesuvius area (elevation contours are drown with grey lines) and distribution of station sites used in this study (open and filled black triangles). Filled triangles indicate the stations used for the calibration of the stochastic procedure. The reference of the map (0;0) corresponds to geographical coordinates Latitude = 40° 49' 52'' N and Longitude = 14° 25' 52'' E. The small insert in the low-right side of the figure shows the location of the investigated area respect to the Italian territory.

Figure 2. Site effect amplification functions for each of the study sites obtained for a 3-sec window at the S wave (from Galluzzo et al., 2006).

Figure 3. T_{RMS} evaluated from the horizontal components of 58 waveforms at the BAF, BKE, SGV and FTC stations. The grey filled squares represent the T_{RMS} evaluated from the observed waveforms by taking the averaged T_{RMS} between the horizontal components of motion. The circles show the T_{RMS} calculated from the envelope of energy flux density for each of the selected earthquakes recorded at the selected sites/stations.

Figure 4. Distance dependence of T_{RMS} evaluated from the energy flux density envelope model for the local earthquakes in the Mt Vesuvius area. The straight black line shows the linear relationship between T_{RMS} and distance obtained by least square fitting.

Figure 5. Observed horizontal acceleration seismograms (top left panels, black-line waveforms) compared to simulated accelerogram (bottom left panel, grey line) for the M_D = 3.6 seismic event of 1999-10-09 recorded at station BKE. Right-hand panels: Corresponding response spectra (5% damping) evaluated from the observed (black lines) and synthetic (grey line, grey fill) waveforms in the frequency range of 1-40 Hz.

Figure 6. Same as for Figure 5, for the M_D = 2.7 seismic event of 1999-11-05 recorded at station SGV.

Figure 7. Same as for Figure 5, for the M_D = 2.6 seismic event of 1999-10-11 recorded at station BKE.

Figure 8. Same as for Figure 5, for the M_D = 3.3 seismic event of 1999-10-11 recorded at station SGV.

Figure 9. Synthetic waveforms and maximum acceleration values evaluated for each of the sites in the Mt Vesuvius area. The values of A_{max} are for an $M_D = 4.3$ seismic event with a stress drop of 70 bar. Maximum values are evaluated by averaging the maximum acceleration from 30 simulated time series. The projection of the fault on the surface is shown by the black rectangle in the center (crater area).

Figure 10. Response acceleration spectra for 5% damping, evaluated for each of the sites for an $M_D = 4.3$ seismic event (stress drop = 70 bar).

Figure 11. Synthetic waveforms and maximum acceleration values evaluated for each of the sites in the Mt Vesuvius area for the $M_D = 5.4$ (stress drop = 70 bar).

Figure 12. Response acceleration spectra for 5% damping, evaluated for each of the sites for an $M_D = 5.4$ seismic event (stress drop = 70 bar).

Tables

Table 1. Scenario earthquake source parameters.

Table 2. Selected earthquake data set parameters (from Del Pezzo et al., 2004). Time and hypocenter coordinates, duration magnitudes and focal parameters of the selected earthquakes.

Table 3. Parameters for the application of the stochastic simulation procedure in the studied area.

Table 4. Fault dimension of selected earthquakes calculated with the Wells and Coppersmith relationship (1994). The "trial and error" calibration procedure between the observed waveforms and the simulated ones is used to set the stress-drop values (column III). The last two columns show the results for the maximum acceleration values evaluated from simulated and observed accelerograms.

Table 5. Maximum acceleration values with standard deviations calculated for each of the sites in the study area. The values of PGA are based on 30 realizations of stochastic simulation. The acceleration values were evaluated for $M_D = 4.3$ and for a stress drop of 60, 70 and 80 bar.

Table 6. Maximum acceleration values with standard deviations calculated for each of the sites in the study area. The values of PGA are based on 30 realizations of stochastic simulation. The acceleration values were evaluated for $M_D = 5.4$ and for a stress drop of 70 bar.